

## Research Article

# Defect detection and repair algorithm for structures generated by topology optimization based on 3D hierarchical fully convolutional network

Zhiyu Wan <sup>a,b</sup>, Hai Lan <sup>b,\*</sup>, Sichao Lin <sup>b</sup>, Houde Dai <sup>b,c,\*</sup>

<sup>a</sup> School of Advanced Manufacturing, Fuzhou University, Jinjiang 362251, China

<sup>b</sup> Quanzhou Institute of Equipment Manufacturing, Haixi Institutes, Chinese Academy of Sciences, Jinjiang 362216, China

<sup>c</sup> Fujian Key Laboratory of Special Intelligent Equipment Safety Measurement and Control, Fujian Special Equipment Inspection and Research Institute, Fuzhou 350008, China

## ARTICLE INFO

## Article history:

Received 30 November 2023

Revised 3 February 2024

Accepted 10 February 2024

Available online 29 February 2024

## Keywords:

Topology optimization

Additive manufacturing

Deep learning

3D semantic segmentation

Defect detection

## ABSTRACT

Customized 3D-printed structural parts are widely used in surgical robotics. To satisfy the mechanical properties and kinematic functions of these structural parts, a topology optimization technique is adopted to obtain the optimal structural layout while meeting the constraints and objectives. However, topology optimization currently faces some practical challenges that must be addressed, such as ensuring that structures do not have significant defects when converted to additive manufacturing models. To address this problem, we designed a 3D hierarchical fully convolutional network (FCN) to predict the precise position of the defective structures. Based on the prediction results, an effective repair strategy is adopted to repair the defective structure. A series of experiments is conducted to demonstrate the effectiveness of our approach. Compared to the 2D fully convolutional network and the rule-based detection method, our approach can accurately capture most defect structures and achieve 89.88% precision and 95.59% recall. Furthermore, we investigate the impact of different ways to increase the receptive field of our model, as well as the trade-off between different defect-repairing strategies. The results of the experiment demonstrate that the hierarchical structure, which increases the receptive field, can substantially improve the defect detection performance. To the best of our knowledge, this paper is the first to investigate 3D defect prediction and repair for topology optimization in conjunction with deep learning algorithms, providing practical tools and new perspectives for the subsequent development of topology optimization techniques.

© 2024 The Author(s). Published by Elsevier B.V. on behalf of Shandong University. This is an open access article under the CC BY-NC-ND license (<http://creativecommons.org/licenses/by-nc-nd/4.0/>).

## 1. Introduction

In recent years, customized and disposable 3D-printed structural parts for surgical robots have been increasingly utilized to meet specific medical requirements [1,2]. Benefitting from the development of high-performance computing resources, automated and intelligent structural optimization techniques have become essential tools for designing 3D-printed structural parts for surgical robots. Structural optimization methods can be classified into size, shape, and topology optimization. Among these methods, topology optimization is widely used in the original design of related structural components because of its advantages, such as no need for an initial design and the minimization of material usage. For example, through topology optimization technology, Sun et al. designed new disposable compatible forceps, which can achieve disposable use of surgical instruments and prevent the spread of

diseases from reusable medical devices [3]. Abdulsalam et al. designed a new bone fixation plate, minimizing the stress shielding phenomenon [4]. Zhang et al. created soft rehabilitation fingers to assist patients in completing rehabilitation training [5]. Currently, the variable density method [6,7], the level set method [8], and the homogenization method [9] are the three main optimization methods for topology optimization. Among them, the variable density method uses pseudo-density to describe the topological solid structure and seeks the optimal force transmission route of the structure, which possesses high computational efficiency and stability and has been applied to commercial optimization software such as ANSYS and Abaqus.

The improvement of design technology has also led to the innovation of manufacturing technology. Additive manufacturing technology (AM), also known as 3D printing, is a manufacturing technology that constructs 3D structures by superimposing materials layer by layer [10]. Over the past decades, molding methods, including stereolithography (SLA) [11], selective laser sintering (SLS) [12], selective laser melting (SLM) [13], and fused deposition

\* Corresponding authors.

E-mail addresses: [lanhai09@fjirsm.ac.cn](mailto:lanhai09@fjirsm.ac.cn) (H. Lan), [dhd@fjirsm.ac.cn](mailto:dhd@fjirsm.ac.cn) (H. Dai).

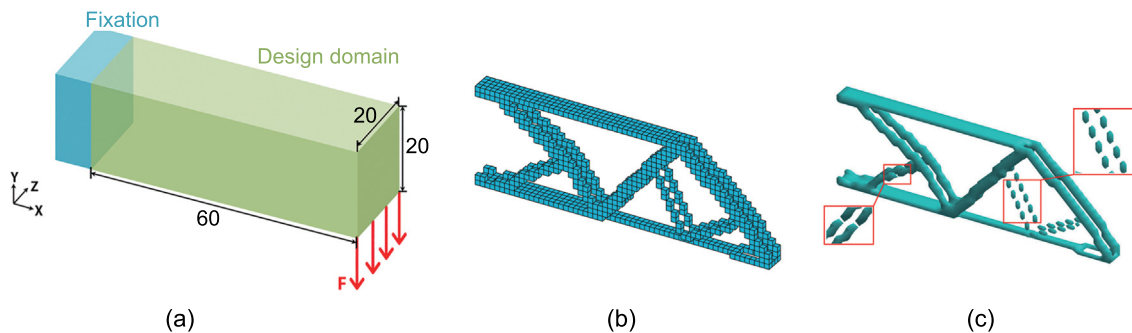


**Fig. 1.** 3D design problem for topology optimization. (a) The 3D design domain and the corresponding loading cases. (b) The structure generated by topology optimization. (c) The STL surface model generated from the voxel structure.

molding (FDM) [14], have emerged [15] and offer a new opportunity to manufacture complex structures. Therefore, additive manufacturing technology has become a common solution to surgical robotic structural component production, allowing developers to focus on improving the performance of the structural components of surgical robots [16]. However, since the variable density method characterizes the topological structure through pseudo-density values, defective structures will appear in the regions with small density values when generating stereolithography files (STL) using the marching cube method. These defective structures must be repaired manually, which is time-consuming, inefficient, and a tremendous obstacle to the practical application of topology optimization technology in the design of structural components. In conclusion, effective defect detection and repair for model structures generated by topology optimization is an urgent challenge.

To address the above problems, Sun et al. proposed a method to repair voxel models by traversing them using a matrix of neighborhood elements [17]. Liu et al. designed a method for clear boundaries of topology optimization results using curve fitting methods [18]. Gorkem et al. proposed a two-stage convolutional network to reduce the number of structural disconnections and decrease pixel errors [19]. However, the above approaches mainly focus on defect repair of 2D-pixel structures or only make preliminary attempts to repair 3D structures. Currently, no end-to-end method exists for detecting and repairing defects in structures generated by topology optimization. Consequently, this paper proposes a deep learning-based method to solve these problems. A series of experimental results proved that the method proposed in this paper can effectively repair the defects generated by topology optimization, which better promotes the application of topology optimization technology in the automated design of structural components for surgical robots.

The main contribution of this paper specifically consists of the following three parts:

- We establish a dataset generated by topology optimization for deep learning model training to address the lack of existing 3D voxel structural datasets. A Matlab topology optimization structure generation module is used to obtain samples by setting different boundaries and constraints. Using connected component analysis and the manual labeling method to mark the position of defective voxels to create a data set for subsequent deep learning algorithm model training.
- In order to effectively detect defects in structures generated by topology optimization, inspired by the success that deep learning algorithms have achieved on image semantic segmentation tasks, a 3D hierarchical fully convolutional

network is designed. This model can effectively detect the defect locations in structures generated by topology optimization, which can provide the basis for the next step of the repair process.

- A simple defect repair scheme based on the neighborhood distance strategy is proposed, which can effectively repair structural defects.

## 2. Data preparation

Currently, no datasets generated by topology optimization in the target detection field can be used for semantic segmentation. We produce a dataset by using the topology optimization simulation framework proposed by Liu Kai et al. [20]. An algorithm for automated labeling of structures generated by topology optimization is also designed.

Topology optimization is based on the basic principles of finite element analysis to achieve the optimal and reasonable distribution of structural materials, which perform best under the given constraints. Its optimization model is shown in Eq. (1):

$$\begin{aligned}
 & \text{find} && \hat{\rho} = [\rho_1, \rho_2, \dots, \rho_e, \dots, \rho_n]^T \\
 & \text{minimize} && c(\hat{\rho}) = F^T U(\hat{\rho}) \quad \text{or} \\
 & && c(\hat{\rho}) = -\mu_{out}(\hat{\rho}) = -L^T U(\hat{\rho}) \\
 & \text{subject to} && v(\hat{\rho}) = \hat{\rho}V - \bar{v} \leq 0 \\
 & && \rho \in \chi, \chi = \{\rho \in \mathbb{R} : 0 \leq \rho \leq 1\}
 \end{aligned} \tag{1}$$

where  $\hat{\rho}$  is a vector consisting of the physical density values of all voxel blocks in the grid of the design area;  $F$  is the vector of nodal forces;  $L$  is a unit length vector with zeros at all degrees of freedom except at the output point where it is one;  $U(\hat{\rho})$  is the vector of nodal displacements;  $v$  is the unit volume of the voxel block.  $V = [v_1, \dots, v_n]^T$  is a vector of element volume, and  $\bar{v}$  is the prescribed volume limit of the design domain.

Fig. 1 provides a graphical illustration of the design problem for the dataset used in this paper and gives an example of the structure generated by topology optimization. In Fig. 1(a), the 3D design domain is the green cuboid with a size of  $20 \times 60 \times 20$  mm. The mesh size and filter radius are set to 1 mm and 1.5 mm, respectively. On the other hand, the fixation region is defined by the blue box in the figure.  $F$  is selected in the range of 1 to 20 N. Young's modulus of the material  $E_0$  is set to 1000 MPa, while Poisson's ratio is set to 0.3. The penalty factor is set to 3, and  $v$  is set to 0.15 to limit the volume of the model. The design process predefined the fixation and force-applying areas as solid-material domains. Different structural optimization models can be obtained by modifying parameters, such as the position of the fixed region, the magnitude of the force, and the direction. Furthermore, to enhance the generalizability of the neural network,

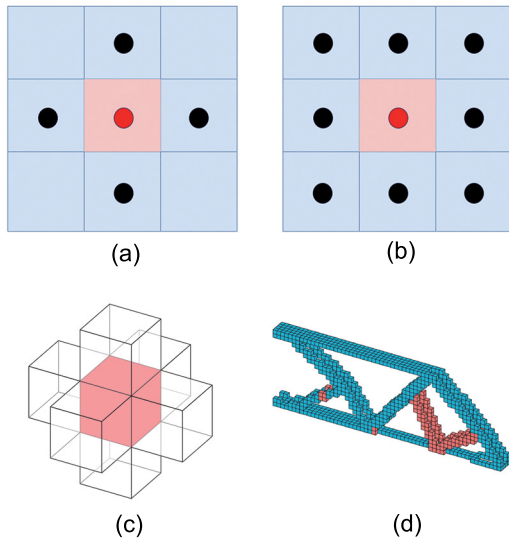


**Fig. 2.** Automated labeling strategy. (a) 4-neighborhood relationships. (b) 8-neighborhood relationships. (c) The neighborhood of 3D voxel. (d) Defects annotation. The blue voxels indicate the normal structure, and the red voxels indicate the defects.

we also used the objective function of the compliance mechanism to generate several samples with different structures.

One of the structures generated according to the above topology optimization method is shown in Fig. 1(b) and (c).

As can be seen from the comparison figure, when transformed into an STL surface model ready for 3D printing, the structure shows defects, thus hindering the practical use of the model.

Currently, software in the industry for labeling structures generated by topology optimization has yet to be created. According to the relevant literature and the dataset analysis in this paper, statistics show that a single shared edge commonly characterizes the regions where the surface model appears to be broken [18]. Most of them have at most one voxel connected in face contact in the surrounding region. We address this situation by designing an automated labeling tool that combines connected component analysis and manual labeling [21].

Connected component analysis refers to finding and labeling connectivity regions in an image, which is commonly used in many application fields, such as CV and image processing, especially in extracting target regions of interest. We use this method to help in the annotation of defects. The typical Connected component analysis is divided into 4-neighbor and 8-neighbor relationship structures, and its connection form is shown in Fig. 2.

Since the samples used in this paper are three-dimensional structures, considering the connectivity characteristics of single shared edges, the adjacency relationship is extended to a 3D 6-adjacency relationship based on Fig. 2(a) for connectivity analysis of structures.

**Algorithm 1:** Algorithm for assisted labeling of voxel model defect structures

```

1 Initialization of  $\hat{\rho} = [\rho_1, \rho_2, \dots, \rho_e, \dots, \rho_n]^T$ ;
2 for  $x_i$  in  $\hat{\rho}$ :
3   if  $x_i = 1$  then
4      $num_1 = \sum_{j \in Neighbor} x_i^{(j)}$ ;
5     if  $num_1 \leq 1$  then
6        $y_i \leftarrow 2$ ;
7   else
8     continue;

```

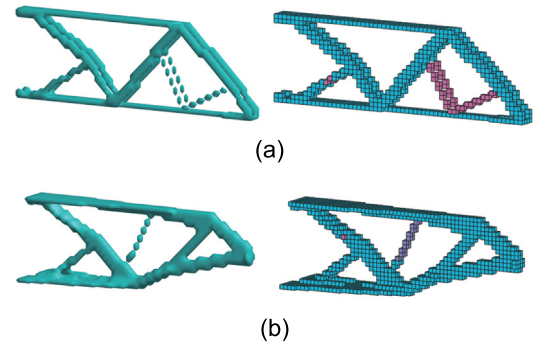


**Fig. 3.** Comparison of labeling results. (a) The structural sample where defects can be detected correctly by the automated labeling tool. (b) The structural sample where defects are not detected correctly. Pink voxels indicate defective voxels labeled by the automated labeling tool, and purple voxels indicate defective voxels need to be labeled manually.

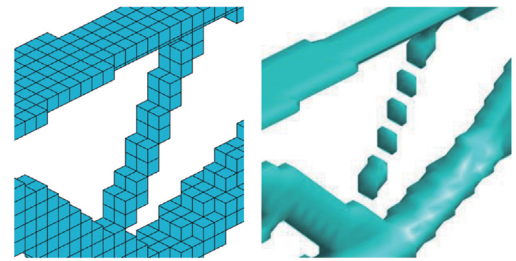


**Fig. 4.** Detail of defective structures not detected by the automated labeling tool.

The 3D connected component analysis algorithm is designed in Algorithm 1, and the 3D defect detection model is shown in Fig. 2(c). In traversing the 3D voxel data, the seed-filling method is used as follows.

(1) Firstly, the structure generated by topology optimization is scanned until it reaches the target voxel point  $B(x, y) == 1$ ;

(2) The target voxel point  $B(x, y)$  is taken as the seed voxel point (the red voxel point in Fig. 2(a)), and then all the voxels in the 3D defect detection model that meet the value of 1 are pressed into the stack;

(3) The number of voxel points in the stack with the value of 1 is counted. If  $num_1 \leq 1$ , it indicates the presence of defects in the vicinity of this voxel point;

(4) Assign a value of 2 to all voxels in the 3D defect detection model that have a value of 1 in this step.

This paper uses the above 3D connectivity analysis algorithm to make an automated labeling tool, which is used to check for possible defects in structures.

The pink voxels in Fig. 3 indicate the possible defective regions given by the automated labeling tool, the purple voxels indicate the defective areas given manually, and the blue voxels indicate the normal structures. In Fig. 3(a) and (b), there are no purple voxels, meaning that defects in this model can be labeled using the automated labeling tool. In contrast, Fig. 3(c) and (d) show that the purple voxels labeled manually appear in the structure much more than those labeled by the automated labeling tool. The results indicate that the automated labeling tool can only accurately label simpler defective structures, such as those shown in Fig. 3(b), but cannot correctly label more complex defects, like those in Fig. 3(d). Fig. 4 shows the defective structures in Fig. 3(d) that the automated labeling tool did not detect. As can be

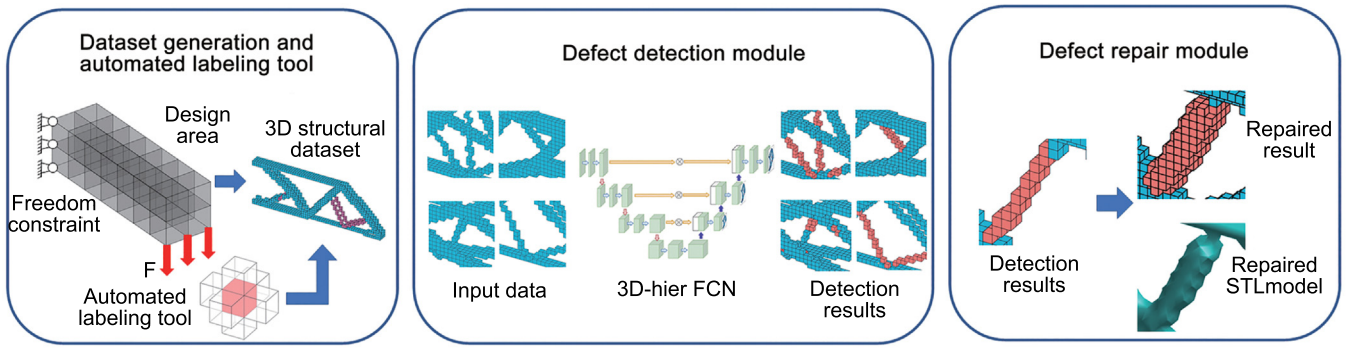


Fig. 5. Holistic framework of defect detection and repair algorithm.

Table 1

Data distribution of a three-dimensional structural dataset.

Data	Label	Amount
Original data	Background voxel	3 730 980
	Normal voxel	253 020
Labeled data	Background voxel	3 730 980
	Normal voxel	248 718
	Defect voxel	4302

seen from the figure, the defective structure consists of multiple voxels side by side, with more than one voxel connected around a defective voxel in the form of facet connections. Therefore, the automated labeling tool did not detect defects. Although the automated labeling tool mentioned above can reduce the workload of manual labeling, it still requires manual improvement of the labeling quality and cannot achieve fully automated detection. Therefore, in this paper, we supplement the automated labeling tool for detecting defects with manual detection to ensure that all defective structures are labeled, effectively improving the quality of data labeling.

The data distribution of the produced dataset is shown in Table 1. In the table, *Original data* represents the density with only two value distributions of 0 and 1. Here, 0 represents the background voxels, and 1 represents the solid voxels. *Labeled Data* includes three distributions of 0, 1, and 2. The meaning of 0 is the same as the original data, while 1 represents the normal voxels and 2 represents the defective voxels. The Table 1 shows that the dataset exhibits a significant data imbalance, with fewer defective voxels than background and normal voxels. This imbalance may result in predicting defective voxels as background or normal structural voxels during deep network training. To solve this problem, data balancing operations must be performed on the network during training.

### 3. Methods

This section describes the method for detecting defects in 3D voxel structures and the strategy for repairing them. Section 3.1 describes the 3D multilayer fully convolutional network used for defect detection, and Section 3.2 describes the strategy used for defect repair. The overall experiment flow is shown in Fig. 5.

#### 3.1. Defect detection model algorithm

##### 3.1.1. 3D hierarchical fully convolutional network

Since the beginning of the 21st century, researchers represented by Hinton et al. [22] introduced the concept of deep learning, and it has made significant progress in target recognition, natural language processing, and semantic segmentation [23].

Among them, FCN [24] is very widely used deep learning network for image semantic segmentation. The model replaces fully connected layers with upsampling and transposed convolutional layers with spatial translation invariance. It also includes a skip connection structure that connects global and local information. The encoder module applies convolutional downsampling to extract high-level abstract features from the data. The decoder then up-samples the feature map output from the encoder through a series of up-sampling and transposed convolutional layers to restore the feature map to the size of the input image. This process enables classification prediction for each pixel while preserving the spatial information in the original input image. The U-Net model [25] and the SegNet models [26] are typical representatives and have achieved outstanding success in video segmentation, medical image segmentation, etc.

Additionally, the attention mechanism is a crucial technique for enhancing the generalization performance of neural networks. It is widely utilized in various deep-learning tasks, including natural language processing, image recognition, and speech recognition. The attention mechanism aims to simulate the selective visual attention mechanism of humans. It focuses the model's attention on a specific part of the input data, selecting critical information for the current task goal while suppressing noise. This improves the model's ability to process and utilize critical information. As the sample's defects are only a small portion of the overall structure, using a network layer that is too deep can result in a loss of spatial detail information. It is essential to maintain a balance between depth and detail. Therefore, we proposed a 3D Hierarchical Fully Convolutional Network (3D-HIER FCN) with a 4-layer encoder-decoder structure, and the skip connection structure is presented in Fig. 6. The downsampling process provides high-level semantic information, while the upsampling process combines spatial structural details through the skip connection structure to obtain more accurate spatial structural information.

##### 3.1.2. Cost function

Table 1 shows the data distribution for the topology optimization dataset. The number of voxels representing the background, normal, and defective structures is obviously imbalanced. The number of normal and defective structure voxels only accounts for 6.24% and 0.11% of the total number, respectively. This imbalance affects the accuracy of segmentation. To accurately identify a small number of defects, we use the class-balanced loss (CB loss) and the dice loss to compose a weighted loss function, CBD loss, for defect detection segmentation. The class-balanced Loss function rebalances the dataset by utilizing the effective number of samples in each class. The effective number of samples is calculated as shown in Eq. (2).

$$E_n = 1 + \lambda \frac{1 - \lambda^{n-1}}{1 - \lambda} = \frac{1 - \lambda + \lambda - \lambda^n}{1 - \lambda} = \frac{1 - \lambda^n}{1 - \lambda} \quad (2)$$

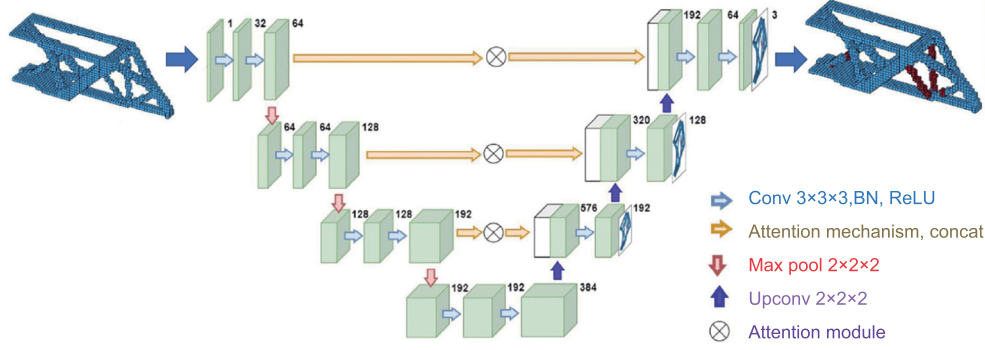


Fig. 6. 3D-HIER FCN for defect detection.

where  $n$  is the number of samples corresponding to each category, the hyperparameter  $\lambda \in [0, 1)$ . The above equation shows that the effective number of samples is an exponential function of the number of samples  $n$ , and  $\lambda$  controls how quickly  $E_n$  grows with  $n$ .

After obtaining effective sample weights for each class, the computational formula for the class balance loss function can be determined based on the weights. Given a sample with label  $y$ , the softmax cross-entropy loss function for that sample is denoted as

$$CE_{softmax}(z, y) = -\log\left(\frac{\exp(z_y)}{\sum_{j=1}^C \exp(z_j)}\right) \quad (3)$$

Suppose class  $y$  has  $n_y$  training samples, and the class equilibrium loss function is denoted as

$$Loss_{CB}(z, y) = -\frac{1-\lambda}{1-\lambda^{n_y}} \log\left(\frac{\exp(z_y)}{\sum_{j=1}^C \exp(z_j)}\right) \quad (4)$$

Dice loss is a regionally correlated loss function, where the loss of the current voxel is associated not only with the predicted value of the current voxel point but also with other voxel points. Utilizing this characteristic can enhance the network's ability to recognize inter-voxel relationships in 3D structures. The formula for calculating Dice loss is defined as

$$Loss_{Dice}(z, y) = 1 - \frac{1}{C} \sum_i^C \sum_j^N \frac{2p_{ij}y_{ij} + \gamma}{p_{ij}^2 + y_{ij}^2 + \gamma} \quad (5)$$

From this, the loss function formula for CB Dice Loss can be obtained as

$$Loss_{cbd} = \alpha Loss_{CB} + \beta Loss_{Dice} \quad (6)$$

where  $\alpha$  and  $\beta$  are the hyperparameters controlling the weights of CB loss and Dice loss in the overall loss function. According to many experiments, it is determined that  $\alpha = 0.8$ ;  $\beta = 1$  is the best hyperparameter value.

The above loss function combines CB Loss and Dice Loss to enhance the network's focus on small samples and gain more insight into the structure of samples. This paper uses CBD Loss in the 3D hierarchical fully convolutional network for defect detection, effectively enhancing the network's detection accuracy.

### 3.2. Repair strategy

After completing defect detection for the structure and verifying the effectiveness of the proposed 3D hierarchical fully convolutional network, an attempt is made to repair the structure based on the results predicted by the neural network.

Automated repair methods for structures are currently lacking in the industry. Typically, repair is done manually in finite

Table 2

Comparison experiment results of defect detection.

Algorithms	Dim	mPrecision	mRecall	mIoU
Automated labeling tool	-	80.32%	83.77%	69.51%
2D FCN	X	89.22%	89.77%	79.53%
	Y	83.02%	85.06%	72.46%
	Z	85.86%	92.34%	80.15%
3D-HIER FCN	-	89.88%	95.59%	86.31%

element analysis software like ANSYS. However, this method can only repair 2D structures. This paper uses the distance analysis method to calculate the distance from the neighborhood voxels in the  $3 \times 3 \times 3$  neighborhood to the center voxel, using the center voxel as the starting point. The neighborhood voxels are then classified into three categories based on the distance size. The distance between the first class of voxels and the center voxel is denoted as 1, which represents the face connection voxel and is noted as the Neighborhood Distance-1 method (ND-1). The distance between the second class of voxels and the center voxel is denoted as  $\sqrt{2}$ , representing the edge connection voxel, and is marked as the ND- $\sqrt{2}$  method. Lastly, the distance between the third class of voxels and the center voxel is denoted as  $\sqrt{3}$ , representing the point-connecting voxel, and is noted as the ND- $\sqrt{3}$  method. Defects are repaired using different combinations of these three types of voxels.

## 4. Experiments

### 4.1. Experimental setup and metrics

For the defect detection experiments, data enhancement operations were performed due to the small number of the dataset and the weak rotational invariance of the convolutional network. The samples are rotated around the X, Y, and Z axes by  $90^\circ$ ,  $180^\circ$ , and  $270^\circ$  to obtain the augmented dataset. The dataset is divided into training and validation sets in an 8:2 ratio, resulting in 266 training samples, 50 validation samples, and 20 test samples.

The network architecture was implemented using PyTorch 2.0.1 and Python version 3.8.18. The training was performed on the NVIDIA GeForce RTX3090 (24G) platform using Adam as an optimizer with a learning rate of  $1 \times 10^{-4}$ . The size of a single input data sample is  $20 \times 60 \times 20$ . The batch size was set to 32 for the training set and 10 for the validation set, resulting in a total of 5000 epochs.

The evaluation metrics for the three categories, background, normal, and defective structures, are recorded separately when different training methods are used. The corresponding metrics of the three categories are then averaged and recorded in Table 2.

$$meval = \frac{1}{C} \sum_{y=0}^C eval^{(y)} \quad (7)$$

where  $meval$  is the average value of a particular evaluation metric;  $C$  is the number of categories in the sample; and  $eval^{(y)}$ , is the value of the evaluation metric predicted by the network for a particular category.

#### 4.2. Defect detection

The proposed 3D hierarchical fully convolutional network is used to evaluate the ability to detect defects in the data-enhanced dataset. Meanwhile, this paper compares the detection results of the automated labeling tool and the 2D fully convolutional network with the method proposed in this paper. The advantages and disadvantages of the three methods in detecting defects are analyzed to validate the effectiveness of the proposed method.

The previous section has already described the principle of the automated labeling tool, so it will not be repeated here. For the 2D fully convolutional network, structural samples are first divided into 2D slices along the X, Y, and Z axes in step of 1. These slices are then used as new 2D training and test datasets. The number of training and test samples generated by cutting along the X and Z directions equals 3320 and 120, respectively. Similarly, cutting along the Y direction generates 9960 training samples and 360 test samples. During training, a 2D fully convolutional network is used to detect defects in each dimension individually. The neural network is trained on a set of training and test samples that are cut along a particular dimension. Table 2 shows the results of comparing the metrics of the three methods.

Due to the high proportion of background and normal voxels in the dataset, the three methods predicted these two types with similar precision and recall metrics of over 95%. Thus, the variations in the average evaluation metrics shown in the table are mainly due to the different results of the methods to predict defects. Table 2 shows that the automated labeling tool has the lowest precision and recall for defect detection and the worst segmentation effect. The 2D fully convolutional network has a higher recall and precision than the first method. However, the structure must be sliced into three independent datasets along each dimension and trained separately to recognize defective structures. This process can be a heavy workload and inefficient. The method proposed in this paper has a slightly higher precision than the 2D fully convolutional network while significantly improving recall compared to other methods. Additionally, it eliminates the need to cut 3D structures into separate 2D datasets, reducing workload while maintaining a high defect detection rate and enabling efficient recognition of defects.

Fig. 7 illustrates the defect detection results of the 3D hierarchical fully convolutional network for various structures generated by topology optimization. Fig. 7(a) displays the Ground Truth of the defects, where blue voxels represent the normal structures, and purple voxels represent the labeled defective structure. Fig. 7(b) shows the predicted results of the defect detection network. Yellow voxels indicate the possible defects predicted by the network. The comparison results in Fig. 7 indicate that most of the defects, which were predicted using the method proposed in this paper, break when converted to STL models. This indicates that the constructed 3D hierarchical fully convolutional network has the ability to detect defects for structures generated by topology optimization.

#### 4.3. Comparison of different repair strategies

The experiments above confirm the effectiveness of the proposed 3D hierarchical fully convolutional network. The network provides defect detection results for the structure. This section creates a defect voxel lookup table by using the coordinates of the defect voxels in the detection results. Then, we attempt to

**Table 3**  
Indicators of defect repair methods.

Repair method	Secondary detection rate	Number of voxels added
ND- $\sqrt{3}$	0	216
ND- $\sqrt{2}$	0	168
ND-1	1.762%	72

repair the structure using the three methods proposed in the previous section. After the repairs were completed, the secondary defect detection rates for each of the three repair methods were calculated separately. The results are presented in Fig. 8.

The secondary detection rates of defects for the three methods are shown in Table 3.

Based on the analysis of structural restoration results and secondary detection rates, when the defect detection network accurately predicts the defects of the model, the ND- $\sqrt{3}$  and ND- $\sqrt{2}$  methods are capable of fully restoring the defects with a secondary detection rate of 0. However, unlike the two repair methods mentioned above, the ND-1 method may introduce new defects while repairing existing ones. Additionally, samples repaired using this method had a secondary defect detection rate of 1.762%. It is essential to consider these potential drawbacks when deciding on a repair method. When comparing the repair effects of the three methods, the number of voxels added to the sample decreases as the neighborhood distance decreases and the damage to the original structure gradually decreases. The results of Fig. 8(c) show that the repaired structure can effectively support the structure, and the ND- $\sqrt{2}$  method effectively reduces shape changes by adding the right amount of voxels. Therefore, based on the above indicators, the ND- $\sqrt{2}$  method is considered optimal for repairing the defects.

#### 4.4. Ablation study on receptive field

This section conducts ablation experiments to verify the effect of spatial structure information in the structure on the network's defect detection capability. The encoder-decoder network structure is replaced with a traditional fully convolutional network (FCN) to detect defects. This change may reduce the ability of the network to acquire contextual information. Meanwhile, defect detection experiments were conducted by setting different sizes of convolutional kernels to compare the network's ability to detect defects under different sensory fields. The network's convolutional kernel sizes were set to 3, 5, 7, 9, and 11 in the experiments. Fig. 9 displays the results of the FCN receptive field experimental network.

The red and blue dashed lines in Fig. 9 represent the precision and recall metrics when training with the 3D hierarchical fully convolutional network, respectively. The solid lines represent the corresponding metrics when FCN detects defects with different convolution sizes.

Comparing the dashed and solid lines shows that without using an encoder-decoder architecture to improve the network's ability to capture contextual information, the FCN network's detection results for the three types of voxels are significantly degraded. These results demonstrate that the detection accuracy and precision of the network can be effectively improved by using a hierarchical network.

Additionally, the solid line shows that the detection accuracy of FCN increases from 79.10% to 81.34% when the convolutional kernel size is increased from 3 to 5. At the convolutional kernel size of 5, the number of background and normal voxels in the receptive field is reasonably increased, reducing the network's

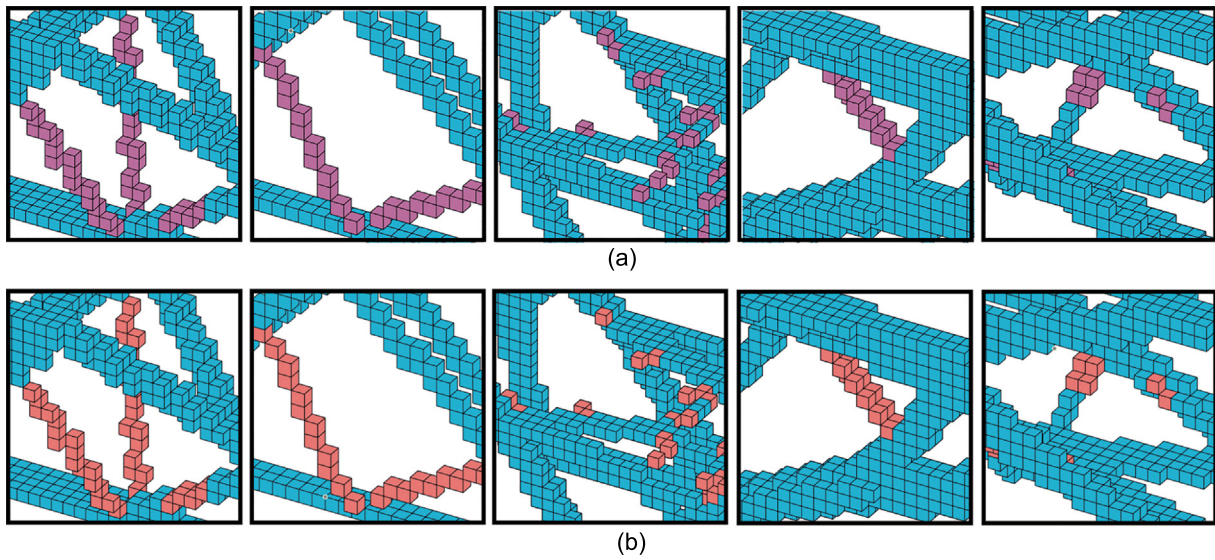


Fig. 7. Comparison of 3D-HIER FCN experimental results. (a) Ground Truth. (b) Results predicted by the 3D-HIER FCN for defect detection.

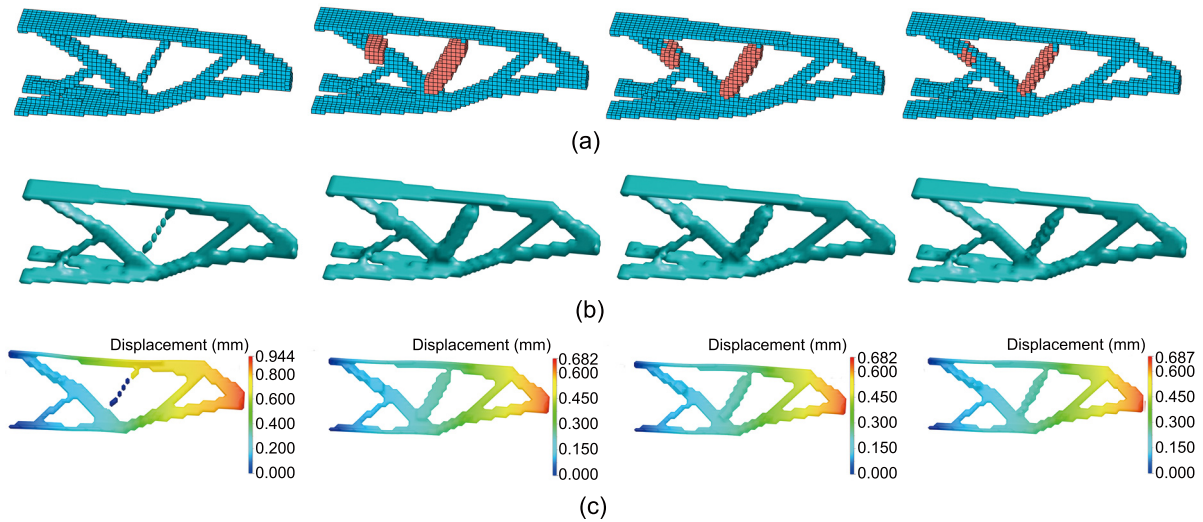


Fig. 8. Comparison of experimental results of different repair strategies. (a) Primitive and repaired voxel structure. (b) STL models. (c) Finite element analysis results of the stl models. The original model is presented in the first column, while columns 2, 3, and 4 show the structures that were repaired by ND-1, ND- $\sqrt{2}$ , and ND- $\sqrt{3}$  methods.

tendency to predict both types of voxels as defects, thus improving accuracy. However, the increase in the number of both types of voxels also increased the network’s prediction error rate for defects. As a result, the recall metric decreased slightly.

As the convolutional kernel continuously increases, the information extracted in the receptive field of the network gradually expands with each convolution. However, the precision and recall of the network segmentation decreases significantly due to the need for a hierarchical structure providing contextual details to support the localization of the extracted features during upsampling. Consequently, the network struggles to effectively complete the defect detection task for structures generated by topology optimization.

### 5. Conclusion

In this paper, we introduce deep learning into the postprocessing of topology optimization simulation results for the first time

in the industry. We also verify the feasibility of combining artificial intelligence methods with automated computer design methods to accomplish structure optimization design. Specifically, we first propose a 3D voxel labeling tool based on neighborhood analysis and use it to produce the first topology optimization dataset generated by topology optimization that can be used for neural network training; then, we propose a 3D hierarchical fully convolutional network to detect defects in structures generated by topology optimization, which achieves effective detection of defective structures. Finally, we propose three defect repair methods based on neighborhood distance analysis for the defect detection results obtained by the network, which initially realizes the repair of defects in structures generated by topology optimization.

With the popularity of topology optimization technology in the design of structural components of surgical robots, the method proposed in this paper can accurately detect and repair structural components when they are defective, thus reducing the workload of manual repair, improving the efficiency of automated

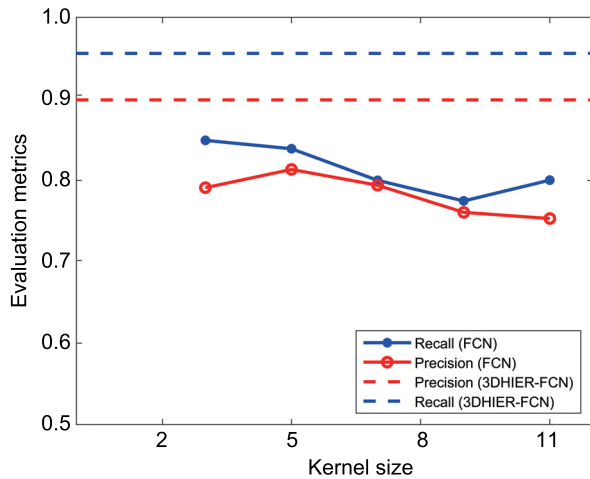


Fig. 9. Results of FCN experiments with different receptive fields.

design of structural components for surgical robots, and meeting the demand for customization. However, the annotation quality of the labeling tool and the sample size of the dataset still need to be improved, as well as the repairing effect of the repairing algorithm. Therefore, in our future work, we will improve the annotation quality of the automated labeling tool and increase the sample size of the dataset. At the same time, we will add the defect detection results into the topology optimization objective function to reduce defective structure generation directly in the topology optimization process.

### Declaration of competing interest

The authors declare that they have no known competing financial interests or personal relationships that could have appeared to influence the work reported in this paper.

### Acknowledgments

This work was supported by the National Natural Science Foundation of China (61973293), the Central Guidance on Local Science and Technology Development Fund of Fujian Province, China (2021L3047 and 2020L3028), the Fujian Provincial Science and Technology Plan Project, China (2021Y0048 and 2021J01388), and the Open Project Program of Fujian Key Laboratory of Special Intelligent Equipment Measurement and Control, Fujian Special Equipment Inspection and Research Institute, China (FJIES2023KF02).

### References

- [1] Theodosia Lourdes Thomas, Venkatasubramanian Kalpathy Venkiteswaran, GK Ananthasuresh, Sarthak Misra, Surgical applications of compliant mechanisms: A review, *J. Mech. Robot.* 13 (2) (2021) 020801.
- [2] Jenna Seetohul, Mahmood Shafiee, Snake robots for surgical applications: A review, *Robotics* 11 (3) (2022) 57.
- [3] Yilun Sun, Yuqing Liu, Lingji Xu, Tim C. Lueth, Design of a disposable compliant medical forceps using topology optimization techniques, in: 2019 IEEE International Conference on Robotics and Biomimetics, ROBIO, IEEE, 2019, pp. 924–929.

- [4] Abdulsalam A Al-Tamimi, Paulo Rui Alves Fernandes, Chris Peach, Glen Cooper, Carl Diver, Paulo Jorge Bartolo, Metallic bone fixation implants: A novel design approach for reducing the stress shielding phenomenon, *Virtual Phys. Prototyp.* 12 (2) (2017) 141–151.
- [5] Hongying Zhang, A. Senthil Kumar, Feifei Chen, Jerry Y.H. Fuh, Michael Yu Wang, Topology optimized multimaterial soft fingers for applications on grippers, rehabilitation, and artificial hands, *IEEE/ASME Trans. Mechatronics* 24 (1) (2019) 120–131.
- [6] M. Zhou, G.I.N. Rozvany, The COC algorithm, part II: Topological, geometrical and generalized shape optimization, *Comput. Methods Appl. Mech. Engrg.* 89 (1) (1991) 309–336, Second World Congress on Computational Mechanics.
- [7] Martin P. Bendsø e, Ole Sigmund, Material interpolation schemes in topology optimization, *Arch. Appl. Mech.* 69 (1999) 635–654.
- [8] Grégoire Allaire, François Jouve, Anca-Maria Toader, A level-set method for shape optimization, *C. R. Math.* 334 (2002) 1125–1130.
- [9] Katsuyuki Suzuki, Noboru Kikuchi, A homogenization method for shape and topology optimization, *Comput. Methods Appl. Mech. Engrg.* 93 (3) (1991) 291–318.
- [10] M. Bhuvanesh Kumar, P. Sathiy, Methods and materials for additive manufacturing: A critical review on advancements and challenges, *Thin-Walled Struct.* 159 (2021) 107228.
- [11] Ferry P.W. Melchels, Jan Feijen, Dirk W. Grijpma, A review on stereolithography and its applications in biomedical engineering, *Biomaterials* 31 (24) (2010) 6121–6130.
- [12] Jean-Pierre Kruth, X. Wang, Tahar Laoui, Ludo Froyen, Lasers and materials in selective laser sintering, *Assem. Autom.* 23 (4) (2003) 357–371.
- [13] Lawrence E Murr, Sara M Gaytan, Diana A Ramirez, Edwin Martinez, Jennifer Hernandez, Krista N Amato, Patrick W Shindo, Francisco R Medina, Ryan B Wicker, Metal fabrication by additive manufacturing using laser and electron beam melting technologies, *J. Mater. Sci. Technol.* 28 (1) (2012) 1–14.
- [14] Sachini Wickramasinghe, Truong Do, Phuong Tran, FDM-based 3D printing of polymer and associated composite: A review on mechanical properties, defects and treatments, *Polymers* 12 (7) (2020) 1529.
- [15] Abishek Kafle, Eric Luis, Raman Silwal, Houwen Matthew Pan, Pratisthit Lal Shrestha, Anil Kumar Bastola, 3D/4D printing of polymers: Fused deposition modelling (FDM), selective laser sintering (SLS), and stereolithography (SLA), *Polymers* 13 (18) (2021) 3101.
- [16] ZHU Jihong, ZHOU Han, WANG Chuang, ZHOU Lu, YUAN Shangqin, Weihong Zhang, A review of topology optimization for additive manufacturing: Status and challenges, *Chin. J. Aeronaut.* 34 (1) (2021) 91–110.
- [17] Yilun Sun, Yuqing Liu, Nandi Zhou, Tim C. Lueth, A matlab-based framework for designing 3d topology optimized soft robotic grippers, in: 2021 IEEE/ASME International Conference on Advanced Intelligent Mechatronics, AIM, IEEE, 2021, pp. 1283–1289.
- [18] Shutian Liu, Quhao Li, Junhuan Liu, Wenjiong Chen, Yongcun Zhang, A realization method for transforming a topology optimization design into additive manufacturing structures, *Engineering* 4 (2) (2018) 277–285.
- [19] Gorkem Can Ates, Recep M. Gorguluarslan, Two-stage convolutional encoder-decoder network to improve the performance and reliability of deep learning models for topology optimization, *Struct. Multidiscip. Optim.* 63 (4) (2021) 1927–1950.
- [20] Kai Liu, Andres Tovar, An efficient 3D topology optimization code written in matlab, *Struct. Multidiscip. Optim.* 50 (2014).
- [21] William E. Lorensen, Harvey E. Cline, Marching cubes: A high resolution 3D surface construction algorithm, in: *Seminal Graphics: Pioneering Efforts that Shaped the Field*, 1998, pp. 347–353.
- [22] Geoffrey E. Hinton, Ruslan R. Salakhutdinov, Reducing the dimensionality of data with neural networks, *Science* 313 (5786) (2006) 504–507.
- [23] Daniel Svozil, Vladimir Kvasnicka, Jiri Pospichal, Introduction to multi-layer feed-forward neural networks, *Chemometr. Intell. Lab. Syst.* 39 (1) (1997) 43–62.
- [24] Jonathan Long, Evan Shelhamer, Trevor Darrell, Fully convolutional networks for semantic segmentation, in: *Proceedings of the IEEE Conference on Computer Vision and Pattern Recognition*, 2015, pp. 3431–3440.
- [25] Olaf Ronneberger, Philipp Fischer, Thomas Brox, U-net: Convolutional networks for biomedical image segmentation, in: *Medical Image Computing and Computer-Assisted Intervention—MICCAI 2015: 18th International Conference, Munich, Germany, October 5–9, 2015, Proceedings, Part III* 18, Springer, 2015, pp. 234–241.
- [26] Vijay Badrinarayanan, Alex Kendall, Roberto Cipolla, Segnet: A deep convolutional encoder-decoder architecture for image segmentation, *IEEE Trans. Pattern Anal. Mach. Intell.* 39 (12) (2017) 2481–2495.